Nanoscale

COMMUNICATION

Cite this: *Nanoscale*, 2014, **6**, 11072

A unique hollow Li_3VO_4/carbon nanotube composite anode for high rate long-life lithium-ion batteries†

Received 6th June 2014
Accepted 29th July 2014

DOI: 10.1039/c4nr03119a

www.rsc.org/nanoscale

Qidong Li,‡ Jinzhi Sheng,‡ Qiulong Wei, Qinyou An, Xiujuan Wei, Pengfei Zhang and Liqiang Mai*

A unique hollow Li_3VO_4/CNT composite is synthesized *via* a facile method as an anode material in lithium batteries. Our work opens up the way for a promising material with high rate capability and good cycling stability due to its efficient Li^+ diffusion and relatively high structure stability.

Introduction

Rechargeable lithium-ion batteries (LIBs) have been one of the most important electrical energy storage technologies for many years, due to their high energy density, low cost and low environmental impact.[1–4] In 2013, five billion LIBs were used to supply power-hungry laptops, cameras, mobile phones and electric cars.[5] Tremendous effort has thus been devoted towards developing high performance LIBs with both high rate performance and high energy density.[6–14] However, graphite, a commercial LIB anode material, cannot meet this high demand for the extensive development of LIBs due to its low ion conductivity (limiting the development of a high rate performance), unsafe conditions (dendritic lithium growth at low potential) and thick solid electrolyte interphase (SEI) layer (which decreases the initial coulombic efficiency).[15–19] There is an urgent need to exploit a high performance and safe anode material for the broader application of LIBs.

State Key Laboratory of Advanced Technology for Materials Synthesis and Processing, WUT-Harvard Joint Nano Key Laboratory, Wuhan University of Technology, Wuhan, 430070, P. R. China. E-mail: mlq518@whut.edu.cn; Fax: +86-027-87644867; Tel: +86-027-87467595

† Electronic supplementary information (ESI) available: The crystal structure of Li_3VO_4; SEM image of hydroxylated CNT; Li_3VO_4 was etched using different dosages of water; TGA curves of Li_3VO_4 and the hollow Li_3VO_4/CNT composite; the production in one pot (360 mL) was weighed to be 3.5237 g; XRD pattern and rate performance of CNT; the capacity contribution ratio of CNTs and the hollow Li_3VO_4; EIS and phase diagram of Li_3VO_4 and Li_3VO_4/CNT after 30 cycles; ECs performance of Li_3VO_4 anode material compared with other previous works. See DOI: 10.1039/c4nr03119a

‡ These authors contributed equally to this work. All authors discussed the results and commented on the manuscript. The authors declare no competing financial interest.

As a promising anode material, $Li_4Ti_5O_{12}$ has been studied as a candidate for LIBs as it has a flat and safe potential (about 1.6 V *vs.* Li^+/Li), and high reversibility upon Li^+ insertion/extraction, along with negligible structure changes.[20–22] However, according to $E = \Delta V \times C$ (E is the energy density, ΔV is the operation voltage of the full cell, C is the capacity), the estimated energy density of $Li_4Ti_5O_{12}$ (regarding both the potential and capacity) would be restricted by the relatively high potential (~1.6 V) and limited theoretical specific capacity (~160 mA h g^{-1}) of the packaged full cell. Lately, $TiNb_2O_7$ with a high theoretical capacity (387 mA h g^{-1}) was reported to be an anode. The performance of $TiNb_2O_7$ had been enhanced to a high level by Guo *et al.* and showed enormous potential to succeed graphite.[23] However, its operation voltage is still high (about 1.2–1.8 V *vs.* Li^+/Li). Therefore, the development of an anode material with both high capacity and a moderate operation voltage would be significant.

Recently, Li_3VO_4 has been investigated as a potential intercalation anode material.[24–26] The potential of Li_3VO_4 during charge and discharge is between 0.5 and 1.0 V (*vs.* Li^+/Li), lower than that of $Li_4Ti_5O_{12}$ and $TiNb_2O_7$, but safer than that of graphite. A considerable theoretical capacity of 394 mA h g^{-1} for Li_3VO_4 is the highest among the above mentioned intercalation anode materials. Li_3VO_4 is built up of oxygen atoms in approximate hexagonal close packing; the cations occupy ordered tetrahedral sites.[27] All of the octahedral sites are empty and interconnected along the *c* axis, forming a fast transmission pathway for Li ions (Fig. S1†). All of these advantages let us regard Li_3VO_4 as a promising anode for the development of high performance LIBs. However, its low electronic conductivity results in poor electrochemical performance (especially poor rate performance), preventing it from being widely used. The common methods used to enhance electronic conductivity are to reduce the particle size or hybridize the material with electronically conductive materials.[28–32] Graphene was used by Shi *et al.* in a hollow Li_3VO_4/G composite,[26] since the hollow structure shortened the ion-diffusion length, while the graphene enabled effective electron transport. This composite showed

good cycle performance and superior rate performance, but the synthesis process was tedious. Therefore, synthesizing Li_3VO_4 with a more effective architecture for high rate performance, *via* a facile and large-scale method remains crucial and challenging.

Herein, we present a unique hollow Li_3VO_4/carbon nanotube (CNT) composite synthesized by a simple, fast and high yield hydrothermal method. The CNTs are connected to construct a three-dimensional (3D) conducting network and bind the hollow Li_3VO_4 (formed by a water etching process) together. This kind of 3D hollow Li_3VO_4/CNT composite is effective for energy storage materials which improves the electrical conductivity and facilitates the penetration of the electrolyte.[33] Different from previous reports, such as the solid-state method[24,25] and long-term hydrothermal process,[26] the Li_3VO_4/CNT composite was synthesized in just two hours, and the unique hollow structure could be easily controlled during the sample washing process. As an anode for LIBs, this hollow Li_3VO_4/CNT composite shows excellent cycle performance (81.7% retention of its 2nd cycle capacity after 2000 cycles at 2 A g^{-1}) and an extremely high rate performance (240 mA h g^{-1} at a high current up to 16 A g^{-1}). The low-cost raw materials, facile synthesis process and high performance make it suitable for mass production.

Experimental section

Sample preparation

First, 4 mmol NH_4VO_3 and 70 mmol LiOH were dissolved in 60 mL deionized water. Then, 70 mg hydroxylated carbon nanotubes (CNTs) were dispersed in the aforementioned solution using magnetic stirring and ultrasound. The resultant mixture was then transferred to a 100 mL Teflon lined autoclave and kept in an oven at 180 °C for 2 h. The product was washed with deionized water and anhydrous ethanol twice, respectively, and dried at 70 °C in a vacuum oven to get the hollow Li_3VO_4/CNT composite. For comparison, a solid Li_3VO_4/CNT composite was prepared using the same procedure, but it was washed just with anhydrous ethanol. Li_3VO_4 was also prepared using the same procedure without the hydroxylated CNTs. The Li_3VO_4/CNT mechanical mixture was prepared by grinding Li_3VO_4 particles and hydroxylated CNTs. The mass ratio between the Li_3VO_4 particles and hydroxylated CNTs was the same as that of the hollow Li_3VO_4/CNT composite.

Material characterization

X-ray diffraction (XRD) data for the samples were collected with a D8 Advance X-ray diffractometer, using Cu Kα radiation (λ = 1.5418 Å) in a 2θ range from 10° to 80° at room temperature. Thermogravimetry/differential scanning calorimetry (TG/DSC) was performed using a Netzsch STA 449C simultaneous thermal analyzer at a heating rate of 10 °C min^{-1} in air. Field emission scanning electron microscopy (FESEM) images were collected with a JEOL-7100F microscope. Transmission electron microscopy (TEM) and high-resolution TEM (HRTEM) images were recorded using a JEM-2100F STEM/EDS microscope. Raman spectra were obtained using a Renishaw INVIA micro-Raman spectroscopy system.

Measurement of electrochemical performance

The electrochemical properties were evaluated by assembling 2016 coin cells in a glove box filled with pure argon gas. The working electrode was prepared by mixing the as-synthesized materials, acetylene black and carboxyl methyl cellulose (CMC) in a weight ratio of 75 : 20 : 5. The slurry was cast onto Cu foil and dried in a vacuum oven at 150 °C for 2 h. The loading of the active materials was 1.2–1.5 mg cm^{-2}. Lithium pellets were used as the anode. The electrolyte was composed of 1 M $LiPF_6$ dissolved in ethylene carbonate (EC)–dimethyl carbonate (DMC) with a volume ratio of 1 : 1. For the Li_3VO_4–$LiFePO_4$ full-cell, the anode was limited and the weight ratio of the cathode to anode was 6.3 : 1. The capacity of the full-cell was calculated based on the mass of the Li_3VO_4 electrode. Galvanostatic charge/discharge measurements were performed using a multichannel battery testing system (LAND CT2001A), and electrochemical impedance spectroscopy (EIS) was carried out with an Autolab Potentiostat Galvanostat. All of the measurements were carried out at room temperature.

Results and discussion

Fig. 1 illustrates the synthesis process for the Li_3VO_4/CNT composite. Ammonium metavanadate (NH_4VO_3) and lithium hydroxide (LiOH) were dissolved in deionized water as precursors. The connection between V and O in solution relates to the pH value. The vanadium exists as a $V_4O_{12}^{4-}$ tetramer in a neutral solution.

The $V_4O_{12}^{4-}$ tetramer will transform to a VO_4^{3-} tetrahedron with the rise in pH value.[34] This process can be shown with the following equations:

$$V_4O_{12}^{4-} + 4OH^- \rightarrow 2V_2O_7^{4-} + 2H_2O \ (13 \geq pH \geq 9) \quad (1)$$

$$V_2O_7^{4-} + 2OH^- \rightarrow 2VO_4^{3-} + H_2O \ (pH \geq 13) \quad (2)$$

Excess LiOH was added to make sure that the vanadium existed in a VO_4^{3-} tetrahedron form. The hydroxylated CNTs were dispersed in the precursor with ultrasonic treatment after the above substances had completely dissolved. Then, the VO_4^{3-} tetrahedrons co-precipitated with Li ions to form Li_3VO_4 particles under hydrothermal treatment. This hydrothermal reaction led to the formation of the Li_3VO_4/CNT composite with an interpenetrating network structure.

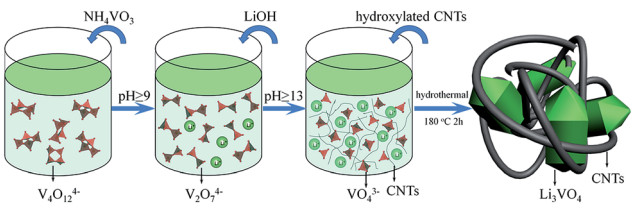

Fig. 1 Schematic of the formation of the Li_3VO_4/CNT composite.

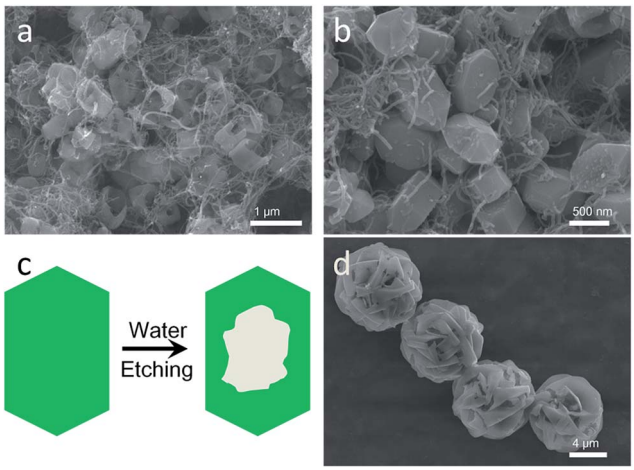

Fig. 2 (a) SEM image of the hollow Li_3VO_4/CNT composite. (b) SEM image of the solid Li_3VO_4/CNT composite. (c) Schematic of the water etching process, from the solid Li_3VO_4 particle to the hollow Li_3VO_4 particle. (d) Li_3VO_4 particles without hydroxylated CNTs during the synthetic process.

A representative SEM image of the hollow Li_3VO_4/CNT composite is shown in Fig. 2a, which exhibits hollow Li_3VO_4 particles confined by the CNT network. An open, screw cap-like hollow structure can be clearly recognized in the composite. The average size of the hollow Li_3VO_4 particles is around 800 nm in length, and 400 nm in width. The wall thickness is around 50–80 nm. The solid Li_3VO_4/CNT particles (Fig. 2b) were washed with water to form the hollow Li_3VO_4/CNT particles, which indicates that water plays a crucial role in this process. Fig. 2c illustrates this etching process. The water etched the Li_3VO_4 particle from one side to the opposite side, to form this screw cap-like hollow structure. This etching process can be ascribed to the selective etching process.[35] The wall thickness of the hollow Li_3VO_4 particles can be controlled by adjusting the time of sample washing as shown as Fig. S3.† This hollow structure is homogeneous and stable, even after the preparation of the electrode (Fig. S4†). The solid Li_3VO_4/CNT particles were washed twice using water to get the hollow Li_3VO_4/CNT composite for consideration of both the electrochemical performance and product production. Without the CNTs, the Li_3VO_4 particle is much bigger than the Li_3VO_4/CNT particle, which consists of many small particles (Fig. 2d). This indicates that the hydroxylated CNTs not only improve the electronic conductivity, but also prevent the aggregation of the Li_3VO_4 particles. TEM and HRTEM were conducted to analyze the Li_3VO_4/CNT composite, as shown in Fig. 3a (before water etching) and Fig. 3b (after water etching). The thickness of the side wall of the hollow Li_3VO_4 particle is about 60 nm (Fig. 3b). HRTEM images (Fig. 3c and d) taken from the front end of the particles clearly show the lattice fringes with a spacing of 3.91 Å, which is in agreement with that of the (011) plane of Li_3VO_4 (JCPDS card no. 38-1247).

Fig. 4a shows the XRD patterns of Li_3VO_4 and the hollow Li_3VO_4/CNT composite. The diffraction peaks can be well

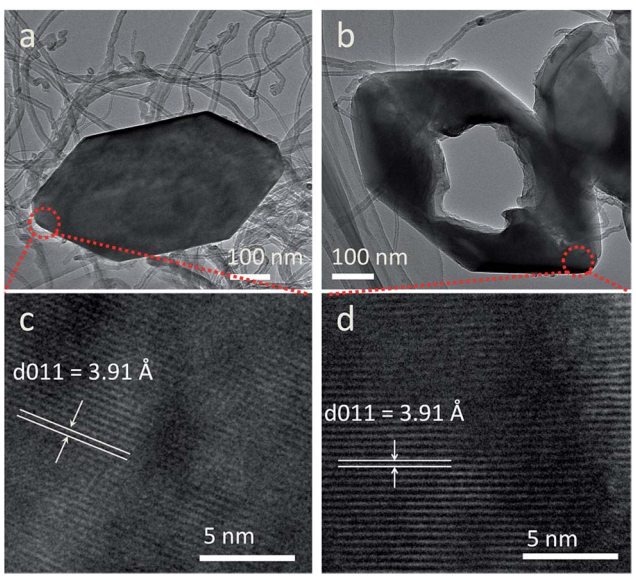

Fig. 3 TEM images further confirm the etching process. (a and c) TEM and HRTEM images of the solid Li_3VO_4/CNT particle. (b and d) TEM and HRTEM images of the hollow Li_3VO_4/CNT particle.

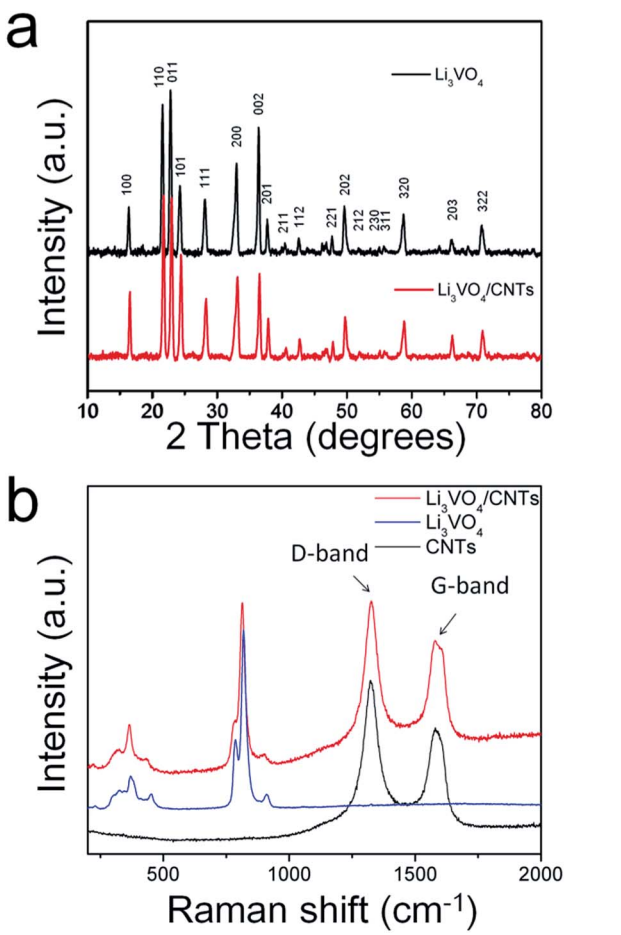

Fig. 4 (a) XRD patterns of the hollow Li_3VO_4/CNT composite and Li_3VO_4. (b) Raman spectra of the hollow Li_3VO_4/CNT composite, Li_3VO_4 and the CNTs.

indexed to an orthorhombic Li_3VO_4 phase (JCPDS card no. 38-1247) with lattice parameters of $a = 5.447$ Å, $b = 6.327$ Å, $c = 4.948$ Å, and $\alpha = \beta = \gamma = 90°$, consistent with a β polymorph with the space group $Pnm2_1$. Diffraction peaks which might appear for the CNTs are absent; most likely the CNT peaks are eclipsed by those for Li_3VO_4. The Raman spectra (Fig. 4b) indicate the existence of Li_3VO_4 and CNTs in the composite. The bands in the ranges of 280–475 cm^{-1} and 750–935 cm^{-1} represent the Li_3VO_4 bands, and the bands in the ranges of 1200–1460 cm^{-1} and 1470–1730 cm^{-1} are attributed to the D-band (*K*-point phonons of A_{1g} symmetry) and G-band (E_{2g} phonons of the C sp^2 atoms) of the CNTs, which confirms the existence of CNTs in the composite. The peak intensity ratio between the peaks at 1333 and 1592 cm^{-1} (I_D/I_G) generally provides a useful index for the degree of crystallinity of various carbon materials, that is, the smaller the I_D/I_G ratio, the higher the degree of ordering in the carbon material.[36] The I_D/I_G values of the hydroxylated CNTs and the hollow Li_3VO_4/CNT composite are 1.375 and 1.233, respectively, indicating an enhancement of the degree of graphitization. The amount of CNTs in the hollow Li_3VO_4/CNT composite was estimated to be approximately 13.76 wt% from thermogravimetric analysis (Fig. S5a†). Our synthetic process is simple and can be easily scaled up. As a demonstration, we performed the reaction in a 500 mL autoclave with 360 mL precursor, and yielded as much as ~3.5 g of product (Fig. S5b†).

Coin cells with lithium as the counter electrode were used to evaluate the electrochemical performance of the as-synthesized materials. All cells were cycled between 0.2 and 3.0 V. Fig. 5a shows the galvanostatic discharge (Li insertion)/charge (Li extraction) profiles for the hollow Li_3VO_4/CNT composite at a low current rate of 0.1 A g^{-1}. The initial discharge capacity is 453 mA h g^{-1} (based on the total weight of the composite), which is higher than the theoretical capacity, because of the formation of the SEI layer. A reversible capacity of 376 mA h g^{-1} can be obtained in the second discharge cycle, which is 83% of the initial capacity.

For practical applications (in full-cell configuration), high current delivery on demand (high rate) is very important. To evaluate the advantages of the hollow and 3D conductive structure, the rate performance was measured at progressively increased current densities (ranging from 0.1 to 16 A g^{-1}) (Fig. 5b and c). It can be seen that the specific capacity of the hollow Li_3VO_4/CNT composite anode is as high as 355, 273 and 265 mA h g^{-1} at 0.1, 4 and 8 A g^{-1}, respectively. Even at a high rate of 16 A g^{-1}, the specific capacity is as high as 240 mA h g^{-1}, which is much higher than that of the Li_3VO_4/CNT mechanical mixture anode (223 mA h g^{-1} at 0.1 A g^{-1}, 146 mA h g^{-1} at 4 A g^{-1}, 130 mA h g^{-1} at 8 A g^{-1} and 110 mA h g^{-1} at 16 A g^{-1}). A comparison of the rate performance with previous work has been shown in Fig. S10 and Table S1.† For the solid Li_3VO_4/CNT composite anode, when the current density is lower than 0.4 A g^{-1}, its capacity is approximately the same as that of the hollow Li_3VO_4/CNT composite. However, when the current density goes up, the capacity gap becomes obvious. The capacity of the solid Li_3VO_4/CNT particles is 140 mA h g^{-1} at 16 A g^{-1},

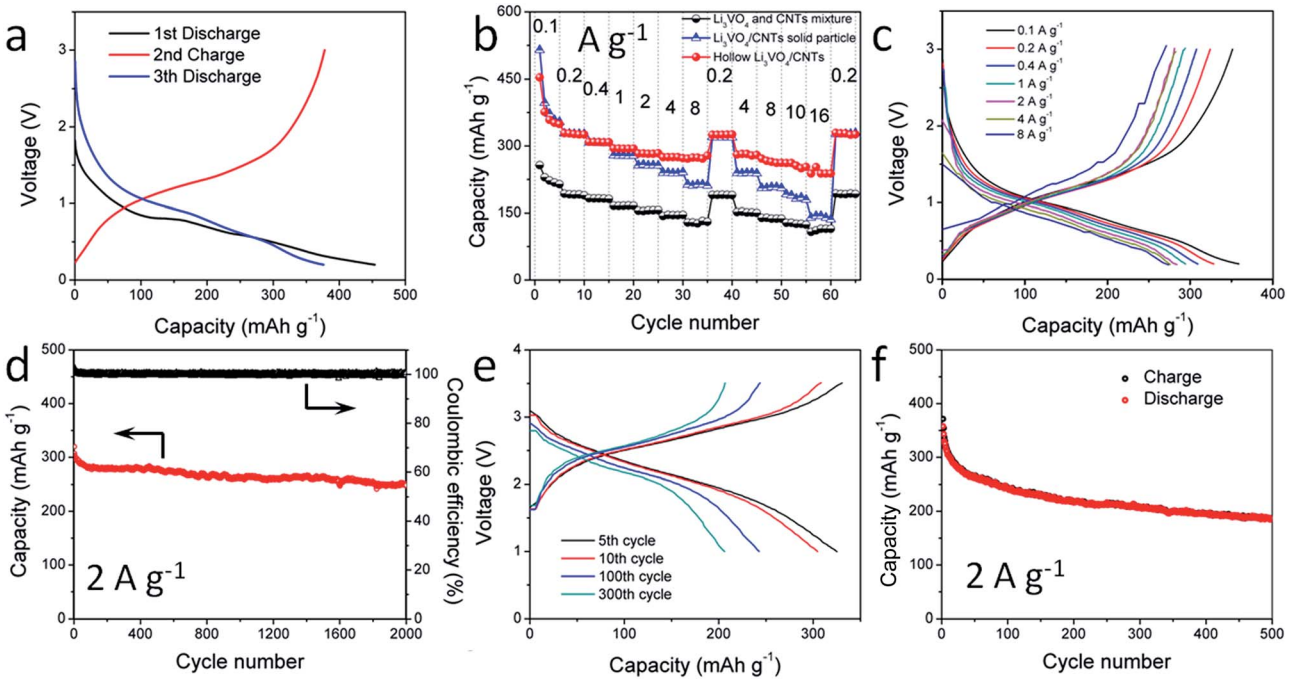

Fig. 5 (a) Typical discharge/charge curves for the hollow Li_3VO_4/CNT composite anode at a current density of 0.1 A g^{-1}. (b) Rate performance of the hollow Li_3VO_4/CNT composite anode, the solid Li_3VO_4/CNT composite anode, and the Li_3VO_4/CNT mechanical mixture anode. (c) Discharge/charge curves for the hollow Li_3VO_4/CNT composite anode at different current densities. (d) Cycle performance of the hollow Li_3VO_4/CNT composite at 2 A g^{-1}. (e and f) Cycle performance and typical discharge/charge curves for the $LiFePO_4$–Li_3VO_4/CNT full-cell at 2 A g^{-1}, with capacity limited by Li_3VO_4/CNT, cycled between 1 and 3.5 V.

100 mA h g^{-1} lower than that of the hollow Li_3VO_4/CNT composite. At 0.1 A g^{-1}, the capacity of the hollow Li_3VO_4/CNT composite is a little lower than that of the solid Li_3VO_4/CNT composite anode, due to the decreased mass ratio of the Li_3VO_4 in the composite from the etching process. To explore the capacity contribution of the CNTs in the composite, coin cells with metallic lithium as the anode were assembled. The rate performance of the hydroxylated CNTs was measured at the same current densities, ranging from 0.1 to 8 A g^{-1} (Fig. S6†). The specific capacity of the CNT anode is 200 mA h g^{-1} at 0.1 A g^{-1}, and 70 mA h g^{-1} at 8 A g^{-1}. Consequently, the actual capacity contribution of the hollow Li_3VO_4 can be calculated to be 393.4 mA h g^{-1} (very close to its theoretical capacity) at 0.1 A g^{-1}, and 306.8 mA h g^{-1} at 8 A g^{-1}. Details of the capacity contribution ratio of each component in the composite are shown in Fig. S7.† Besides excellent rate capability, the hollow Li_3VO_4/CNT composite has a superior long cycle performance at high current density. The hollow Li_3VO_4/CNT composite shows very good stability at 2 A g^{-1}, and 250 mA h g^{-1} is still obtained even after 2000 cycles (81.7% retention of its 2nd cycle capacity) (Fig. 5d).

The electrochemical impedance spectrum (EIS) was used to provide further insight (Fig. S8†). The EIS spectrum shows two compressed semicircles from the high to medium frequency range of each spectrum, which describes the charge transfer resistance (R_{ct}) for these electrodes, and a line inclined at approximately 45° in the low-frequency range, which could be considered as Warburg impedance (Z_W). After simulating the second compressed semicircle for both samples, the values of R_{ct} for the Li_3VO_4 and the hollow Li_3VO_4/CNT electrodes after 30 cycles were calculated to be 354.5 and 24.04 Ω, respectively. This result suggests that the hollow Li_3VO_4/CNT composite has faster kinetics for Li ion insertion/extraction.[37–39]

The high rate capability and excellent cycling stability observed for the hollow Li_3VO_4/CNT composite can be ascribed to the interconnected 3D conductive framework and the unique hollow structure as mentioned above. First, the CNTs prevent the agglomeration of Li_3VO_4 particles to reduce the particle size, which increases the contact area between Li_3VO_4 and the electrolyte.[31] Li_3VO_4 particles are wrapped by the CNTs, and the CNTs connect together to form a 3D conductive structure at the same time, which greatly improves the conductivity.[40–42] This promotes the electrochemical performance comprehensively. Second, the unique open hollow structures provide more sites for Li ion transportation, reduce the diffusion distance for Li ions, and buffer the local volume change during Li^+ insertion/extraction, leading to high stability and good charge/discharge performance at large current density.[43] The above favorable properties clearly show that the hollow Li_3VO_4/CNT composite is a very promising candidate for practical applications in LIBs.

Full-cells combining the commercial $LiFePO_4$ cathode with our hollow Li_3VO_4/CNT anode have been assembled. Fig. 5e shows charge/discharge curves for the Li_3VO_4/CNT–$LiFePO_4$ full cell at 2 A g^{-1} (7 min full charge or discharge). According to its respective voltage, the full cell gives an operating voltage of around 2.5 V. Its capacity is above 300 mA h g^{-1} for the first few cycles, and 185 mA h g^{-1} after 500 cycles (Fig. 5f). The capacity fading of the full cell is 45% after 500 cycles, very close to that of the commercial $LiFePO_4$ (42%) (Fig. S9†). In addition, the capacity fading of $LiFePO_4$ and the hollow Li_3VO_4/CNT composite is 0.107% and 0.0275% per cycle, respectively, which indicates that the capacity fading of the full cell is limited by the commercial $LiFePO_4$.

Conclusions

A Li_3VO_4/CNT composite is synthesized *via* a facile, low cost and rapid hydrothermal method. The Li_3VO_4 nanoparticles could be further etched by water, resulting in the hollow structure. The hollow Li_3VO_4/CNT composite exhibited extremely high rate performance and a long cycle life, which is demonstrated by over 2000 cycles with a capacity of 250 mA h g^{-1} at 2 A g^{-1}. Even at 16 A g^{-1}, 240 mA h g^{-1} can still be obtained. This excellent electrochemical performance is attributed to the connected CNT 3D conductive framework and the hollow structure. Meanwhile, this time-saving and easy-to-operate approach can be easily used for mass production. Furthermore, a 2.5 V full cell couple was assembled with a commercial $LiFePO_4$ cathode that had a good high rate performance, which demonstrates the prospect of its application in rapid charge/discharge LIBs. Therefore, it is shown that this hollow Li_3VO_4/CNT composite can be a promising anode material for high performance and low-cost LIBs.

Acknowledgements

This work was supported by the National Basic Research Program of China (2013CB934103), the International Science & Technology Corporation Program of China (2013DFA50840), the National Science Fund for Distinguished Young Scholars and the Fundamental Research Funds for the Central Universities (2013-VII-028, 2014-YB-001). Thanks to Prof. C. M. Lieber of Harvard University and Prof. Dongyuan Zhao of Fudan University for strong support and stimulating discussions.

Notes and references

1 B. Kang and G. Ceder, *Nature*, 2009, **458**, 190.
2 B. Dunn, H. Kamath and J.-M. Tarascon, *Science*, 2011, **334**, 928.
3 H. Wu, G. Chan, J. W. Choi, I. Ryu, Y. Yao, M. T. McDowell, S. W. Lee, A. Jackson, Y. Yang and L. Hu, *Nat. Nanotechnol.*, 2012, **7**, 310.
4 H. Zhang, X. Yu and P. V. Braun, *Nat. Nanotechnol.*, 2011, **6**, 277.
5 R. V. Noorden, *Nature*, 2014, **507**, 26–28.
6 M. Armand and J.-M. Tarascon, *Nature*, 2008, **451**, 652–657.
7 C. K. Chan, H. Peng, G. Liu, K. McIlwrath, X. F. Zhang, R. A. Huggins and Y. Cui, *Nat. Nanotechnol.*, 2008, **3**, 31–35.
8 L. J. Fu, H. P. Zhang, Q. Cao, G. J. Wang, L. C. Yang and Y. P. Wu, *Microporous Mesoporous Mater.*, 2009, **117**, 515–518.
9 T. Xia, W. Zhang, J. Murowchick, G. Liu and X. B. Chen, *Nano Lett.*, 2013, **13**, 5289–5296.

10 Y. S. Hu, X. Liu, J. O. Müller, R. Schlögl, J. Maier and D. S. Su, *Angew. Chem.*, 2008, **48**, 210–214.
11 J. J. Xu, H. Y. Wu, F. Wang, Y. Y. Xia and G. F. Zheng, *Adv. Energy Mater.*, 2013, **3**, 286–289.
12 C. Wang, W. Wan, Y. H. Huang, J. T. Chen, H. H. Zhou and X. X. Zhang, *Nanoscale*, 2014, **6**, 5351–5358.
13 Y. Yao, N. Liu, M. T. McDowell, M. Pasta and Y. Cui, *Energy Environ. Sci.*, 2012, **5**, 7927–7930.
14 H. Wu, G. Yu, L. Pan, N. Liu, M. T. McDowell, Z. Bao and Y. Cui, *Nat. Commun.*, 2013, **4**, 1943.
15 S. S. Zhang, K. Xu and T. R. Jow, *J. Power Sources*, 2006, **160**, 1349–1354.
16 S. S. Zheng, *J. Power Sources*, 2006, **161**, 1385–1391.
17 G. J. Wang, J. Gao, L. J. Fu, N. H. Zhao, Y. P. Wu and T. Takamura, *J. Power Sources*, 2007, **174**, 1109–1112.
18 H.-K. Kim, S.-M. Bak and K.-B. Kim, *Electrochem. Commun.*, 2010, **12**, 1768–1771.
19 D. Aurbach, B. Markovsky, I. Weissman, E. Levi and Y. Ein-Eli, *Electrochim. Acta*, 1999, **45**, 67–86.
20 T. Ohzuku, A. Ueda and N. Yamamoto, *J. Electrochem. Soc.*, 1995, **142**, 1431–1435.
21 J. Chen, L. Yang, S. Fang, S.-i. Hirano and K. Tachibana, *J. Power Sources*, 2012, **200**, 59–66.
22 E. Kang, Y. S. Jung, G. H. Kim, J. Chun, U. Wiesner, A. C. Dillon, J. K. Kim and J. Lee, *Adv. Funct. Mater.*, 2011, **21**, 4349–4357.
23 B. K. Guo, X. Q. Yu, X. G. Sun, M. F. Chi, Z. A. Qiao, J. Liu, Y. S. Hu, X. Q. Yang, J. B. Goodenough and S. Dai, *Energy Environ. Sci.*, 2014, **7**, 2220–2226.
24 W.-T. Kim, Y. U. Jeong, Y. J. Lee, Y. J. Kim and J. H. Song, *J. Power Sources*, 2013, **244**, 557–560.
25 H. Q. Li, X. Z. Liu, T. Y. Zhai, D. Li and H. S. Zhou, *Adv. Energy Mater.*, 2013, **3**, 428–432.
26 Y. Shi, J. Z. Wang, S. L. Chou, D. Wexler, H. J. Li, K. Ozawa, H. K. Liu and Y. P. Wu, *Nano Lett.*, 2013, **13**, 4715–4720.
27 A. R. West and F. P. Glasser, *J. Solid State Chem.*, 1972, **4**, 20.
28 Q. L. Wei, Q. Y. An, D. D. Chen, L. Q. Mai, S. Y. Chen, Y. L. Zhao, K. M. Hercule, L. Xu, A. M. Khan and Q. J. Zhang, *Nano Lett.*, 2014, **14**, 1042–1048.
29 S. Li, Y. F. Dong, L. Xu, X. Xu, L. He and L. Q. Mai, *Adv. Mater.*, 2014, **26**, 3545–3553.
30 X. L. Ji, K. T. Lee and L. F. Nazar, *Nat. Mater.*, 2009, **8**, 500–506.
31 W. Tang, Y. Y. Hou, X. J. Wang, Y. Bai, Y. S. Zhu, H. Sun, Y. B. Yue, Y. P. Wu, K. Zhu and R. Holze, *J. Power Sources*, 2012, **197**, 330–333.
32 F. X. Wang, S. Y. Xiao, Y. Y. Hou, C. L. Hu, L. L. Liu and Y. P. Wu, *RSC Adv.*, 2013, **3**, 13059–13084.
33 Z. Chen, Y. Yuan, H. H. Zhou, X. L. Wang, Z. H. Gan, F. S. Wang and Y. F. Lu, *Adv. Mater.*, 2014, **26**, 339–345.
34 J. Livage, *Chem. Mater.*, 1991, **3**, 578–593.
35 C. H. Kuo and M. H. Huang, *J. Am. Chem. Soc.*, 2008, **130**, 12815–12820.
36 X. L. Wu, L. Y. Jiang, F. F. Cao, Y. G. Guo and L. J. Wan, *Adv. Mater.*, 2009, **21**, 2710–2714.
37 L. Q. Mai, B. Hu, W. Chen, Y. Y. Qi, C. S. Lao, R. S. Yang, Y. Dai and Z. L. Wang, *Adv. Mater.*, 2007, **19**, 3712.
38 X. Xu, Y. Z. Luo, L. Q. Mai, Y. L. Zhao, Q. Y. An, L. Xu, F. Hu, L. Zhang and Q. J. Zhang, *NPG Asia Mater.*, 2012, **4**, e20.
39 L. Q. Mai, Q. L. Wei, Q. Y. An, X. C. Tian, Y. L. Zhao, X. Xu, L. Xu, L. Chang and Q. J. Zhang, *Adv. Mater.*, 2013, **25**, 2969–2973.
40 X. L. Jia, Z. Chen, A. Suwarnasarn, L. Rice, X. L. Wang, H. Sohn, Q. Zhang, B. M. Wu, F. Wei and Y. F. Lu, *Energy Environ. Sci.*, 2012, **5**, 6845–6849.
41 Z. Chen, V. Augustyn, X. L. Jia, Q. F. Xiao, B. Dunn and Y. F. Lu, *ACS Nano*, 2012, **6**, 4319–4327.
42 Z. Chen, J. W. F. To, C. Wang, Z. D. Lu, N. Liu, A. Chortos, L. J. Pan, F. Wei, Y. Cui and Z. N. Bao, *Adv. Energy Mater.*, 2014, DOI: 10.1002/aenm.201400207.
43 X. W. Lou, L. A. Archer and Z. C. Yang, *Adv. Mater.*, 2008, **20**, 3987–4019.